Effect of Calcination Temperature on Physical properties of Ni0.6Zn0.4Fe2O4 Ferrite nanoparticles

sivakumar pendyala (sivakumar.pendyala@gmail.com)
Malla Reddy Engineering College https://orcid.org/0000-0002-3119-3189
G.k.Sivasankara Yadav
Rayalaseema University

Manuscript (Regular Article)

Keywords: Sol-gel auto combustion, LCR, VSM and Dielectric constant

Posted Date: February 1st, 2021

DOI: https://doi.org/10.21203/rs.3.rs-167748/v1

Abstract

The influence of Calcination temperature on the physical properties of $Ni_{0.6}Zn_{0.4}Fe_2O_4$ ferrite nanoparticles were investigated. These ferrite nanoparticles have been synthesized by sol-gel auto combustion method using citric acid as fuel agent at different calcination temperatures (400^0C, 500^0C and 600^0C). The Morphological investigation, average crystallite size and microstructure of the material were examined by using X-ray diffraction (XRD) and confirmed by field emission scanning electron microscope (FESEM) and FTIR spectra. The Effects of calcination temperature on the dielectric and magnetic properties were calculated by using LCR meter and vibrating sample magnetometer (VSM). The XRD result shows a single-phase cubic spinel structure with average crystallite size increases from 27 to 29.5 nm, with an increase of temperature. The highest saturation magnetization was found at a calcination temperature 600^0C with value 80.39 emu/g, and the value coercive field (H_c) was inverse with the crystallite size.

1. Introduction

The spinel ferrites have concerned much attention in recent years due to their exceptional magnetic, electrical properties and chemical stabilities [1–3]. Nanoscale $NiFe_2O_4$ is one of the versatile and technologically important soft ferrite materials with significant qualities such as low coercivity, high electrical resistivity and chemical stabilities, catalytic behaviour, etc. Because of these properties, $NiFe_2O_4$ nanoparticles have various potential applications in magnetic fluids, electrodes, catalysis, sorbent, gas sensor, and biomedicine [4–8]. In general, the spinel ferrites attained a chemical formula is AB_2O_4, where ‘A’ and ‘B’ can indicate the tetrahedral and octahedral sites, respectively. In other words, the divalent cations such as Ni^{+2}, Mg^{+2}, Zn^{+2}, Co^{+2}, Cu^{+2} and Mn^{+2} can occupy the A-site while the B site can be occupied by trivalent cation like Fe^{+3} [9, 10]. For example, $NiFe_2O_4$ and $ZnFe_2O_4$ can exhibit a cubic spinel structure [11, 12]. Nevertheless, these spinel structures will be again classified into three types (normal spinel, inverse spinel and mixed spinel) based on the degree of inversion ($0 < \delta < 1$). The $\delta = 1$, $\delta = 0$ and $\delta = 0.25$ for normal spinel, inverse spinel and mixed spinels, respectively [13]. Normally, the degree of inversion was inter-linked to the cation distribution between A and B-sites. This cation distribution was observed to be different for bulk and nano ferrites. Both Ni and Zn ferrites are known to have a dominant preference for tetrahedral and octahedral locations, whereas nickel ferrite is an inverse spinel ferrite and zinc ferrite is a normal spinel ferrite. The composite Ni – Zn ferrites, however, are known to exist as a completely mixed spinel structure. The variation of elemental composition in these ferrites results in the redistribution of metal ions over the tetrahedral and octahedral sites, which can alter the properties of ferrites. The properties of these ferrite nanoparticles can also be tailored by altering parameters such as doping concentration or the synthesis process [14]. Because of this NiZn ferrites are prepared and studied for distinct physical properties.

2. Experimmental

The chemical formula of considered Mg-doped Zn ferrite is $Ni_{0.6}Zn_{0.4}Fe_2O_4$ was prepared using the sol-gel auto combustion method. All used precursors are nitrates provided by Merck and Sigma Aldrich chemicals with AR grade having 99.5% purity. Magnesium nitrate [$Ni(NO_3)_2$ $6H_2O$], zinc nitrate [$Zn(NO_3)_2$ $6H_2O$], ferrous nitrate [$Fe(NO_3)_3$ $9H_2O$] are precursors and citric acid [$C_6H_8O_7$ H_2O] act as burning agent and ammonia solution (NH_3) is for maintaining the pH level of solution. The nitrates were dissolved using distilled water separately in a glass beaker. They were mixed into a large beaker using magnetic stirrer after the individual chemicals had been fully dissolved. After some time a clear solution was formed, maintain citric acid to nitrate ratio as 1:3 by adding two solutions. From the previous works of literature, we consider 1:3 molar ratio is suitable for obtaining less agglomeration and tiny sized particles. Maintaining pH value equal to 7 by adding ammonia (NH_3) drop by drop under constant stirring. The previous works of literature also indicate that the size of the particles depends on the pH value. After a few hours, during the stirring and heating stage observed the homogenous solution. By continuous heating and stirring at 150°C, water molecules evaporated continuously after some time a dense and extremely sticky gel was found.

This gel was heated in the temperature range180^0C-220^0C. After some time, evapourate the water molecules completely, at the time of instant observe the burning of gel automatically give rise to auto combustion, it is very quick due to the evolution of gaseous products. Moreover, after a while, the full gel transformed to ashes or smouldered, "erupting like a volcano from the lower of the beaker to the upper. This process was completed in no moment. The obtained powders colures in dark brown ash were produced at temperature 250^0C in the form of a tree structure. Finally, the powder was cooled to room temperature. The complete preparation steps are shown in Fig. 1 The agate mortar is used to grind the powder for 30 minutes, then samples are obtained in the form of incredible dense.

Finally obtained powder specimen is calcinated under standard circumstances at temperature 400^0C, 500^0C and 600^0C about 4 hours and maintain room temperature. Also, all prepared powder samples are tested for structural analyses, using various techniques XRD, SEM and EDS. VSM is used for magnetic study and LCR meter for dielectric study.

3. Results And Discussion

3.1 XRD Analysis

Figure(2) illustrate XRD pattern of synthesized $Ni_{0.6}Zn_{0.4}Fe_2O_4$ nano ferrite calcinated at 400^0C, 500^0C and 600^0C respectively. The XRD pattern of $Ni_{0.6}Zn_{0.4}Fe_2O_4$ ferrite shows eight peaks situated in a range of 20^0 to 80^0 angle. The peak intensity equivalent to a structure is displayed in terms of % of miller indices as shown in Fig. (2). The obtained X-ray diffraction pattern suitable with JCPDS card no.10–325. There was a change in the Zn ferrite structure with the addition of Ni content [15].

The pattern of $Ni_{0.6}Zn_{0.4}Fe_2O_4$ can be indexed as a pure cubic spinel structure and found to the presence of secondary phases. The doping of Ni content, extra peaks arises corresponding to the nickel composition as indicating with the "♦" symbol shown in figure(2) [15]. The most intense (311) peak of cubic spinel ferrite observed as a measure of its degree of good crystallinity. The crystallite size (D) of $Ni_{0.6}Zn_{0.4}Fe_2O_4$ sample was calculated by using the Scherrer formula is given by

$$D = \frac{0.9\lambda}{\beta COS\Theta}$$

1

Where k = 0.9 is Scherrer's constant, λ = 1.5406 Å is the wavelength of the incident x-rays, β is the full width at half maximum (FWHM) of diffraction peak, and θ is the Bragg's angle of diffraction.

Figure (3) shows the variation of crystallite size with an increase of calcination temperature. The crystallite size (D) varies from 27.07 to 29.42 nm. The observed variation in the crystallite size is mainly due to that agglomeration of nanoparticles[16]Unlike crystallite size, the lattice parameter values decrease with the increase of calcination temperature.

The decreasing nature of lattice parameter values is due to the less ionic radii of Ni^{2+} (0.69Å) ions substituted in place of large ionic radii of Zn^{2+} (0.74Å) at tetrahedral sites at all calcination temperatures, as shown in Fig. (3). A similar type of behaviour was observed by Ashok Kumar in nickel Zinc ferrites. [17]

The lattice parameter (a) of $Ni_0.6Zn_{0.4}Fe_2O_4$ nanoparticles is determined by using equation

$$a = d\sqrt{h^2 + k^2 + l^2}$$

2

3.2 SEM Analysis:

The SEM analysis is used to study the morphology of all the samples. Figure (4) shows SEM micrographs of $Ni_{0.6}Zn_{0.4}Fe_2O_4$ specimen. All micrographs showed the same magnifications. From the SEM images, it can be found that synthesized samples contain nanoparticles. Hence, the prepared nanoparticles look like spherical, dispersed and less agglomeration. From SEM study, the observations on grain size reveal that increasing nature with an increase of calcination temperature and changed like the XRD analysis.

3.3 EDS ANALYSIS

Figure 5 shows the EDS spectrum for $Ni_{0.6}Zn_{0.4}Fe_2O_4$ nano ferrite samples. EDS is one of the powerful tools for describing the percentage of elemental composition in the sample. Table 2. shows the list of elemental and atomic percentages of samples. All images indicate the presence of elements used for synthesizing such as atoms of Ni, Zn, Fe, and oxygen. No other impurity components present in the [illegible] prepared samples are defect-free and homogenous.

Table 1

Dependence of crystallite size (D), lattice constant (a)and unit cell volume (a^3) of $Ni_0.6Zn_{0.4}Fe_2O_4$ nanoparticles

Composition (X)	Calcination temperature (^0C)	Crystallite size D(nm)	Lattice constant a (Å)	Volume of the Unit cell a^3 (Cm^3)
$Ni_{0.6}Zn_{0.4}Fe_2O_4$	400	26.97	8.36065	584.41
	500	28.3	8.35933	584.13
	600	29.48	8.35643	583.52

Table 2

Elemental and atomic percentages of $Ni_{0.6}Zn_{0.4}Fe_2O_4$

Element	O		Ni		Zn		Fe	
Concentration (x)	Element %	Atomic %	Element %	Atomic %	Element %	Atomic %	Element %	Atomic %
0.6	26.24	56.25	13.26	6.62	11.62	6.1	45	27.64

3.4 FTIR Analysis:

Figure 6. illustrates IR spectra for $Ni_{0.6}Zn_{0.4}Fe_2O_4$ nano ferrite specimens calcined at 400^0C, 500^0C and 600^0C in the range between 400 to 900 cm^{-1} at 300K. The IR studies provide data about the structural formation of the spinel ferrite. The observed band positions from IR results as shown in Table 3. IR results indicate two prominent bands around 600 and 400 cm^{-1} in all samples due to vibrations of tetrahedral and octahedral sites [18]. Hence, confirm the prepared samples having a single phase with a homogenous structure.

Table 3

FTIR band positions of $Ni_{0.6}Zn_{0.4}Fe_2O_4$ at 400^0C, 500^0C and 600^0C calcination temperatures.

Concentration (X)	Calcination temperature (^0C)	Higher Frequency band (v_1) cm^{-1}	Lower Frequency band (v_2) cm^{-1}
$Ni_{0.6}Zn_{0.4}Fe_2O_4$	400	576.32	418.09
	500	574.42	420
	600	557.41	420

Table.4: Dependence of M_s, M_r and H_c values of $Ni_{0.6}Zn_{0.4}Fe_2O_4$ ferrite nanoparticles at 400^0C, 500^0C and 600^0C

CalciationTemprature	Composition	M_s(emu/g)	M_r(emu/g)	H_c(Oe)
400^0C	$Ni_{0.6}Zn_{0.4}Fe_2O_4$	61.077	12.28	338
500^0C		70.25	14.03	268
600^0C		80.7978	16.37	224

The observed frequency bands (v_1) in the range of 557 to 577 cm^{-1} are considered as the high-frequency bands (strong absorption), whereas the frequency bands (v_2) in the range of 418 to 420 cm^{-1} are considered to be the low-frequency bands (weak absorption). The increase in calcination temperature causes an increase in the high-frequency bands and lower frequency bands [19]. The Ni^{2+} ions substituted at (A) site, shifting the proportional number of Fe^{2+} ion from A to B site, causes to enhance in the cation-oxygen bond length of tetrahedral lattice site (A) of spinel ferrite

3.5 Dielectric Properties

The behaviour of dielectric constant (K) with ln(f) in the frequency range 1Hz to 1MHz for $Ni_{0.6}Zn_{0.4}Fe_2O_4$ calcined at 400^0C, 500^0C and 600^0C as shown in Fig. 7. The dielectric constant (K) of Ni-doped Zn ferrite at 300k has been measured by using formula 3. All the samples are sintered at 800^0C. The values of dielectric constant (K) decrease with increasing the frequency. At a certain frequency, the observed dielectric constant is unchanged and independent on frequency, possess normal behaviour of ferromagnetic material.

$K = C\,d / \varepsilon_o\,A$ (3)

K---- is dielectric constant

d----- thickness of the sample

A---- Area of the sample

C----- capacitance of a capacitor with a dielectric

Effect of frequency on dielectric constant

The dielectric constant (K) described based on the Maxwell–Wagner type of interfacial polarization that has an adequate agreement with Koop's theory [20]. Ferrites comprise of conducting grain with weak grain boundaries. Initially, the electrons follow the applied field and piled up at the grain boundaries through the exchange mechanism that forms polarization. However, at a specific frequency, the hopping

of electrons between Fe^{2+}/Fe^{3+} ions can not follow the field, and it consumes a definite time to align in the field direction that triggers to reduce the polarization. Hence the dielectric constant decreases.

Figure 7. illustrates the changing of dielectric constant with increasing frequency calcined at 400^0, 500^0C and 600^0C. The enhancement of dielectric constant with calcination temperature is mainly due to that more Ni^{2+} ions occupy A sites instead of Fe^{3+} ions. Hence, the number of Fe^{3+} ions migrate to B site, causes more concentration of $Fe^{3+} \leftrightarrow Fe^{2+}$ ion pairs at the B-site and consequently the amount of space charge polarization increases, leads to increase the values of dielectric constant [21].

3.6 Magnetic properties:

Figure 8 indicates the M-H curves of $Ni_{0.6}Zn_{0.4}Fe_2O_4$ sample analyzed at room temperature using a vibrating sample magnetometer with a maximum field of ± 15 (kOe) calcinated at 400^0C, 500^0C and 600^0C. The derived values of saturation magnetization (Ms), residual magnetization (M_r) and coercivity (H_c) are mentioned in table 4. It can be observed that the values of the saturation magnetization Ms and remanent magnetization Mr are increased by increasing the temperature from 400^0C to 600^0C, which arising from spin non-colinearity at the surface of the crystals. The changes in the magnetic properties of the nanoparticles can be attributed to the modification of the crystallinity and crystallite size dependent on the calcination temperature. The variation of coercivity Hc was not in accordance with that of Ms and Mr, indicating that Hc was not determined only by the size of nanoparticles [22, 23].

4. Conclusions:

In summary, effects of calcination temperature on the physical properties and crystallinity of $Ni_{0.6}Zn_{0.4}Fe_2O_4$ ferrite nanoparticles successfully synthesized by sol-gel auto combustion method have been investigated with the aim of the dependence of physical properties on the crystallite size and expanding the range of applications. Our results showed that the dielectric constant and magnetic properties of the $Ni_{0.6}Zn_{0.4}Fe_2O_4$ nanoparticles were strongly affected by the calcination temperature as a consequence of the gradual increase in the crystallinity and particle size. Therefore, ideal magnetic properties and behaviour of $Ni_{0.6}Zn_{0.4}Fe_2O_4$ nanoparticles can be achieved by changing the calcination temperature.

Declarations

Acknowledgements

The author greatly indebted to Authors are thankful to *Dr Panthagani Raju*, Department of Physics, Osmania University, Hyderabad, India, for his support to carry out the LCR measurements.

Conflict of Interest:

No conflict of interest in this paper

References

1. Deng H, Li XL, Peng Q, Wang X, Chen JP, Li YD (2005) Monodisperse magnetic single-crystal ferrite microspheres. Angew Chem Int Ed 44,:2782–2785. DOI:10.1002/anie.200462551
2. Pervaiz E, Gul IH, and H. Anwar:" Hydrothermal synthesis and characterization of CoFe2O4 nanoparticles and nanorods", J Supercond Nov Magn. 26 (2013) 415–424. https://link.springer.com/article/10.1007/s10948-012-1749-0
3. Bellusci M, Canepari S, Ennas G, Barbera AL, Padella F, Santini A, Scano A, Seralessandri L, Varsano F: "Phase evolution in the synthesis of manganese ferrite nanoparticles", J Am Ceram Soc. 90: (2007), 3977–3983. **https://doi.org/10.1111/j.1551-2916.2007.02061.x**
4. Laurent S, Forge D, Port M, Robic C, Elst VL, Muller RN (2008) " Magnetic iron oxide nanoparticles: synthesis, stabilization, vectorization, physicochemical characterizations, and biological applications". Chem Rev 108:2064–2110. https://doi.org/10.1021/cr068445e
5. Feng SJ, Yang W, Wang ZB (2011) Synthesis of porous $NiFe_2O_4$ microparticles and its catalytic properties for methane combustion. Mater Sci Eng B 176:1509–1512. 10.1016/j.mseb.2011.09.007
6. Jacob J, Khadar MA, "Investigation of mixed spinel structure of nanostructured nickel ferrite", J Appl Phys 107 (2010). 114–310. https://doi.org/10.1063/1.3429202
7. Zak T, Saed D, Aman D, Younis SA, Moustafa YM, "Synthesis and characterization of MFe_2O_4 sulfur nano adsorbents", J Sol-Gel Sci Technol65(2013) 269–276. DOI:10.1007/s10971-012-2933-1
8. L.Satyanarayana KM, Reddy, Sunkara VM (2003) Nanosized spinel $NiFe_2O_4$: a novel material for the detection of liquefied petroleum gas in air. Mater Chem Phys 82:21–26. https://doi.org/10.1016/S0254-0584(03)00170-6
9. Naresh U, Kumar RJ, Naidu KCB (2019) Optical, magnetic and ferroelectric properties of $Ba_{0.2}Cu_{0.8-x}La_xFe_2O_4$ (x = 0.2–0.6) nanoparticles. Ceram Int 45:7515–7523. https://doi.org/10.1016/j.ceramint.2019.01.044
10. Naresh U, Kumar RJ, Naidu KCB (2019) Hydrothermal synthesis of barium copper ferrite nanoparticles: nanofiber formation, optical, and magnetic properties. Mater Chem Phys 236:121807. https://doi.org/10.1016/j.matchemphys.2019.121807
11. Taha TA, Azab AA, Sebak MA (2019) Glycerol-assisted sol-gel synthesis, optical, and magnetic properties of $NiFe_2O_4$ nanoparticles. J Mol Struct 1181:14–18. https://doi.org/10.1016/j.molstruc.2018.12.075
12. KUMAR PS, THYAGARAJAN K, KUMAR AG, "Investigations on physical properties of Zn ferrite nanoparticles using sol-gel auto combustion technique", Digest Journal of Nanomaterials and Biostructures. 13(4)(2018)P.P 1117–1122. https://www.chalcogen.ro/1117_PendyalaSK.pdf
13. Naidu KCB, Madhuri W (2017) Hydrothermal synthesis of $NiFe_2O_4$ nanoparticles: structural, magnetic properties. Bull Mater Sci 40:417–425. DOI

10.1007/s12034-017-1374-4

14. AbuEl-Fadl A, Hassan AM, TetianaTatarchuk MHMahmoud, Yaremiy IP, Gismelssed AM, Ahmed MA (2019) Synthesis and magnetic properties of spinel $Zn_{1-x}Ni_xFe_2O_4$ ($0.0 \leq x \leq 1.0$) nanoparticles synthesized by microwave combustion method". journal of Magnetisam Magnetic materials 471:,192–199. https://doi.org/10.1016/j.jmmm.2018.09.074
15. Sheikh AD, Mathe ÆVL, "Anomalous electrical properties of nanocrystalline Ni–Zn ferrite", J Mater Sci, 43 (2008) 2018–2025. https://link.springer.com/article/10.1007/s10853-007-2302-6
16. Singh RPreetP, Hudiara IS, Rana SB (2016) Effect of calcination temperature on the structural, optical and magnetic properties of pure and Fe-doped ZnO nanoparticles. Materials Science-Poland 34(2):451–459. DOI:10.1515/msp-2016-0059
17. Kumar A, Kumar P, Rana G, Yadav MS, Pant RP (2015) A study on structural and magnetic properties of $Ni_xZn_{1-x}Fe_2O_4$ ($0 \leq x \leq 0.6$) ferrite nanoparticles. Appl Sci Lett 1(2):33–36. DOI:10.17571/appslett.2015.01009
18. Maaz K, Mumtaz A, Hasanain SK, Ceylan A (2007) Synthesis and magnetic properties of cobalt ferrite $CoFe_2O_4$ nanoparticles prepared by wet chemical route. J Magn Magn Mater 308:289–295. https://doi.org/10.1016/j.jmmm.2006.06.003
19. Khot SS, Shinde NS, Ladgaonkar B, Kale BB, Watawe SC, "Effect of temperature of synthesis on X-Ray, IR properties of Mg-Zn ferrites Prepared by Oxalate Co-Precipitation Method", International Journal of Advances in Engineering & Technology (2011) 2231 – 1963. DOI: 10.4028/www.scientific.net/KEM.547.57
20. Wagner KW (1913) Zur Theorie der unvolZkomvn6nem Dielektrilza. Ann Phys 40:817–855. https://doi.org/10.1002/andp.19133450502
21. Pendyala SK, Thyagarajan K, Guru Sampath A Kumar & Obulapathi L (2019) " Investigations on physical properties of Mg ferrite nanoparticles for microwave applications". Journal of microwave power electromagnetic energy 3(1):3–11. https://doi.org/10.1080/08327823.2019.1569898
22. Sivakumar P, Ramesh R, Ramanand A, Ponnusamy S, Muthamizhchelvan C (2011) Synthesis and characterization of $NiFe_2O_4$ nanosheet via polymer assisted co-precipitation method. Mater Lett 65:483–485. https://doi.org/10.1016/j.matlet.2010.10.056
23. Mohallem NDS, Seara L (2003) Magnetic nanocomposite thin films of $NiFe_2O_4/SiO_2$ prepared by sol-gel process. Appl Surf Sci 214:143–150. https://doi.org/10.1016/S0169-4332(03)00304-0

Figures

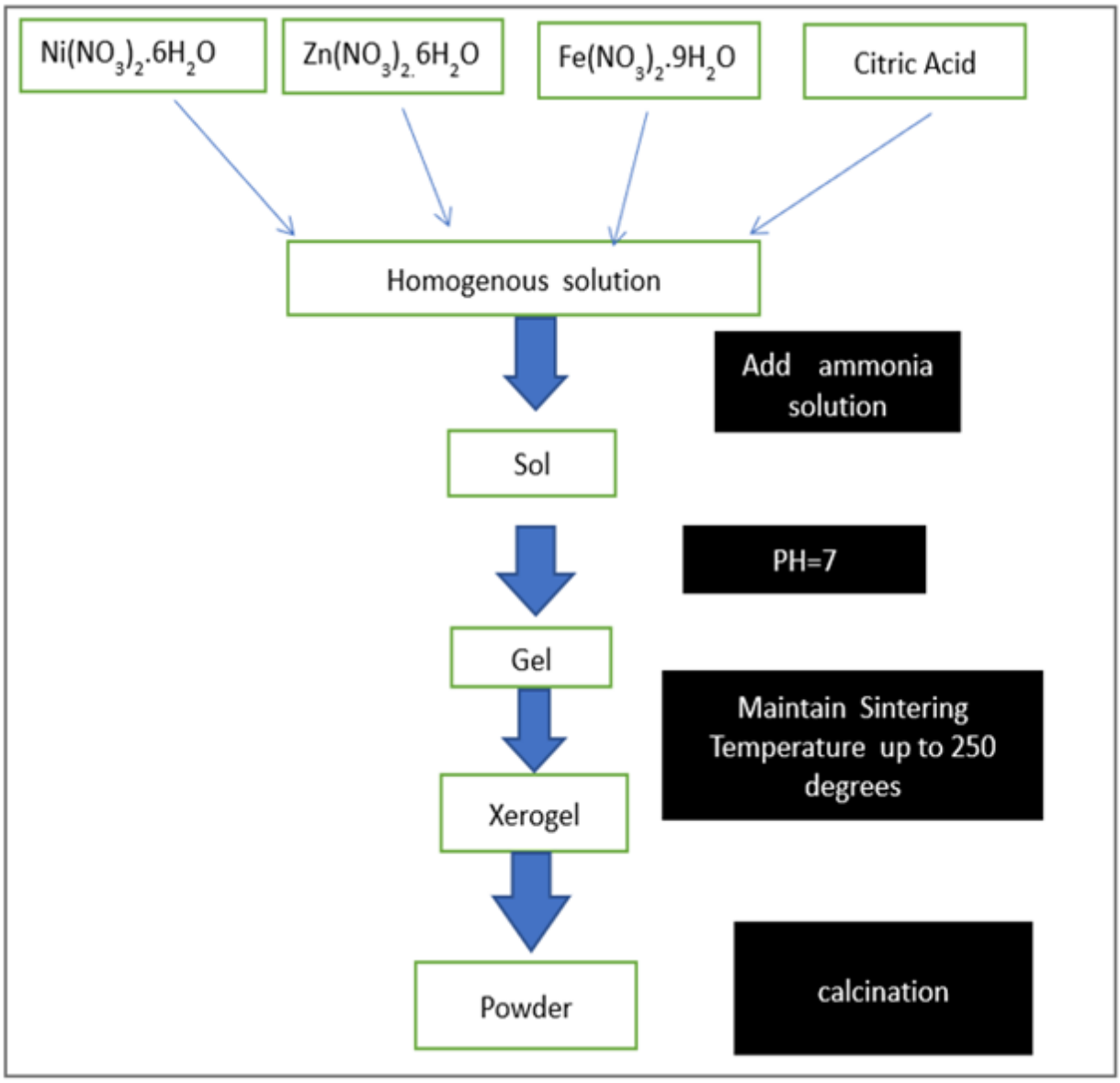

Figure 1

Flow chart synthesis process of Ni-doped Zn Nanoparticles

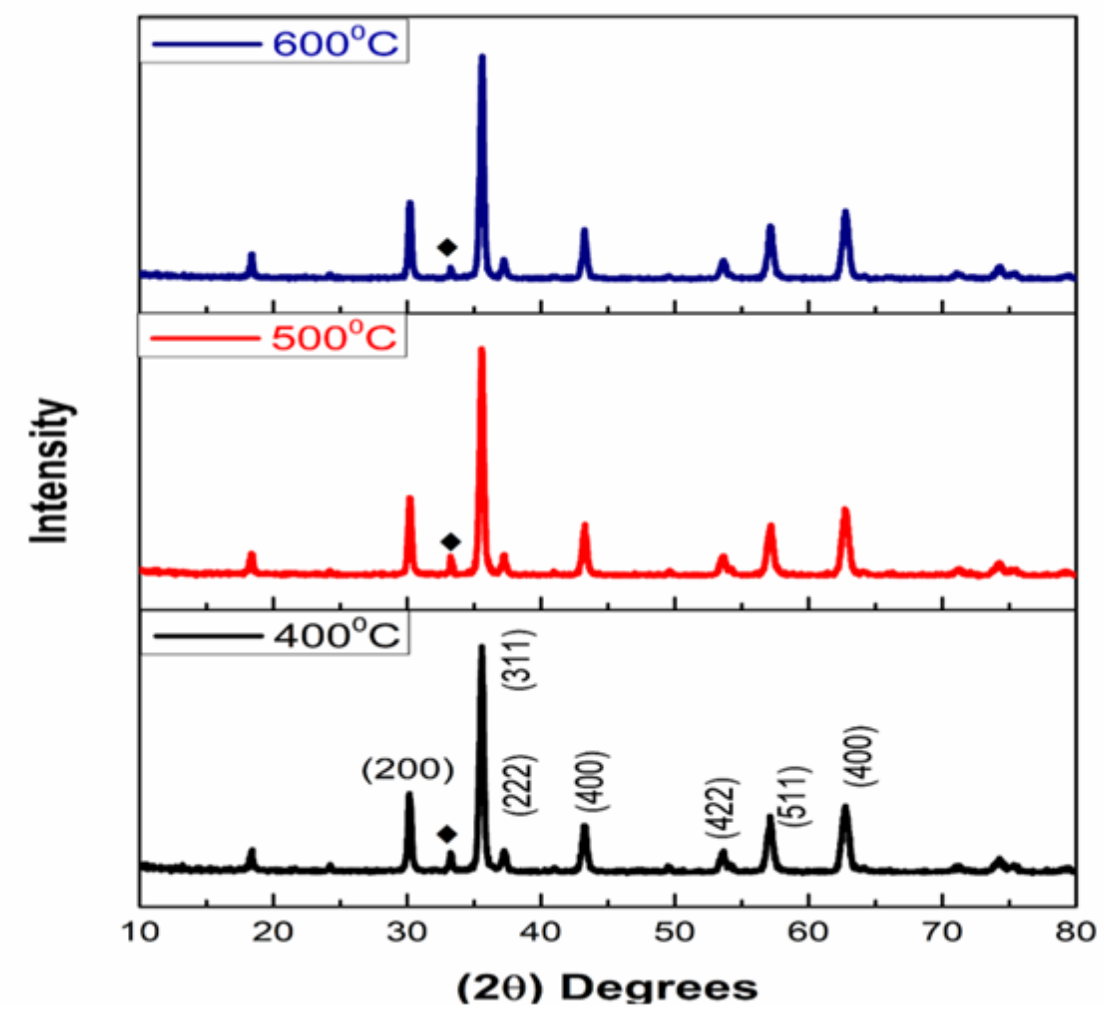

Figure 2

XRD pattern of Ni0.6Zn0.4Fe2O4 nanoparticles calicined at 4000C, 5000C and 6000C

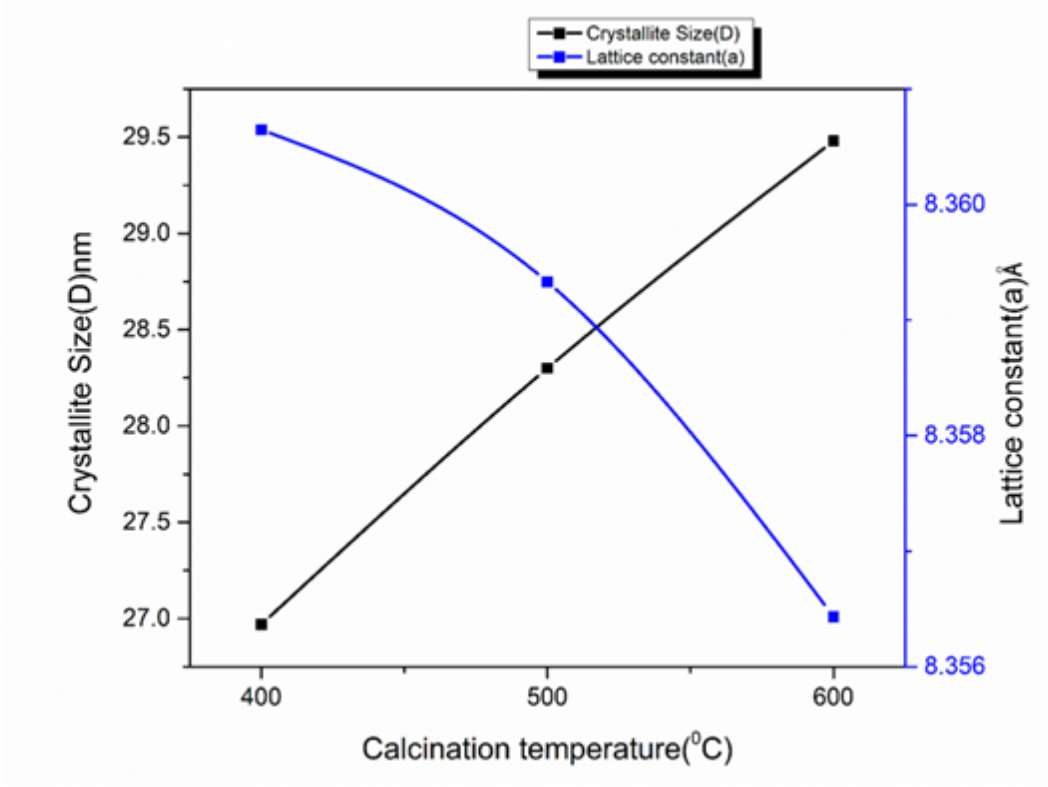

Figure 3

Variation of crystallite size and lattice constant of Ni0.6Zn0.4Fe2O4 ferrite nanoparticles at 4000C, 5000C and 6000C calcination temperatures

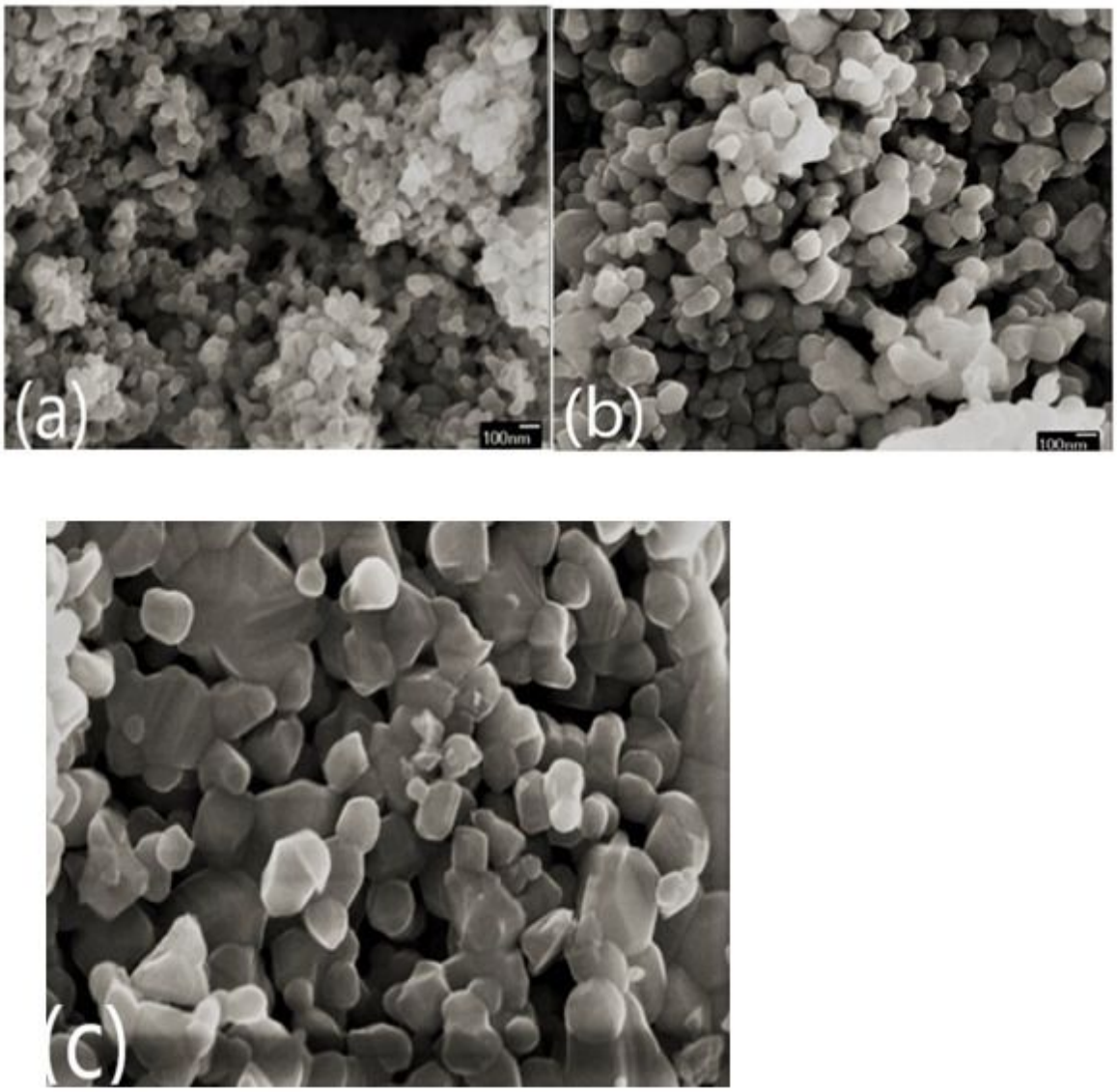

Figure 4

(a,b&c): SEM micrographs of Ni0.6Zn0.4Fe2O4 ferrite nanoparticles at 4000C, 5000C and 6000C calcination temperatures.

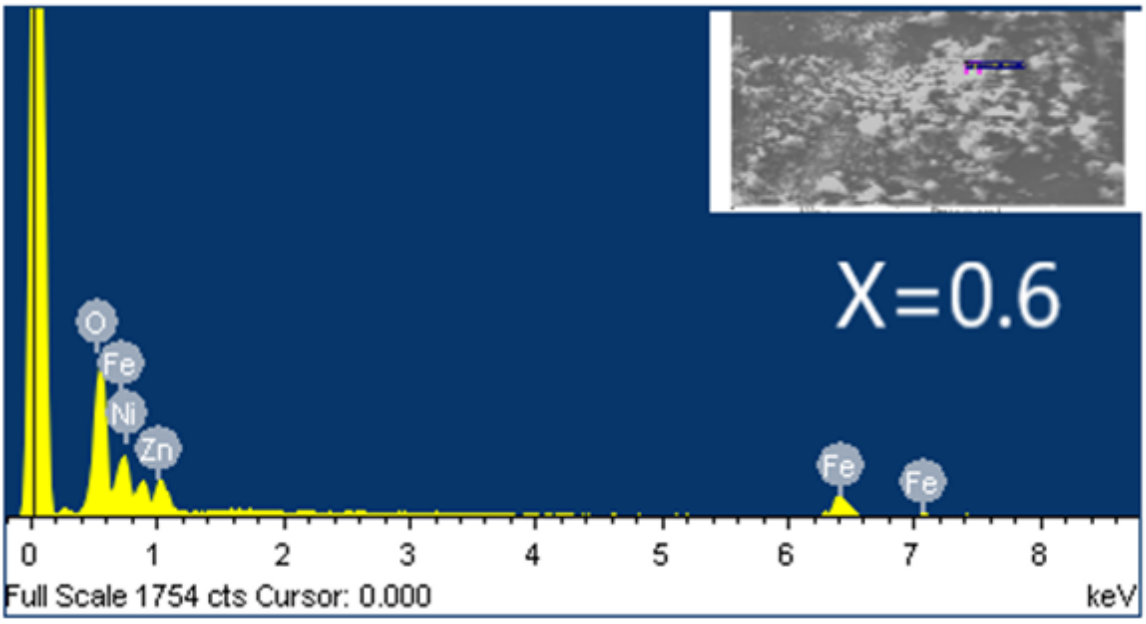

Figure 5

EDS image for Ni0.6Zn0.4Fe2O4 nano ferrite particles.

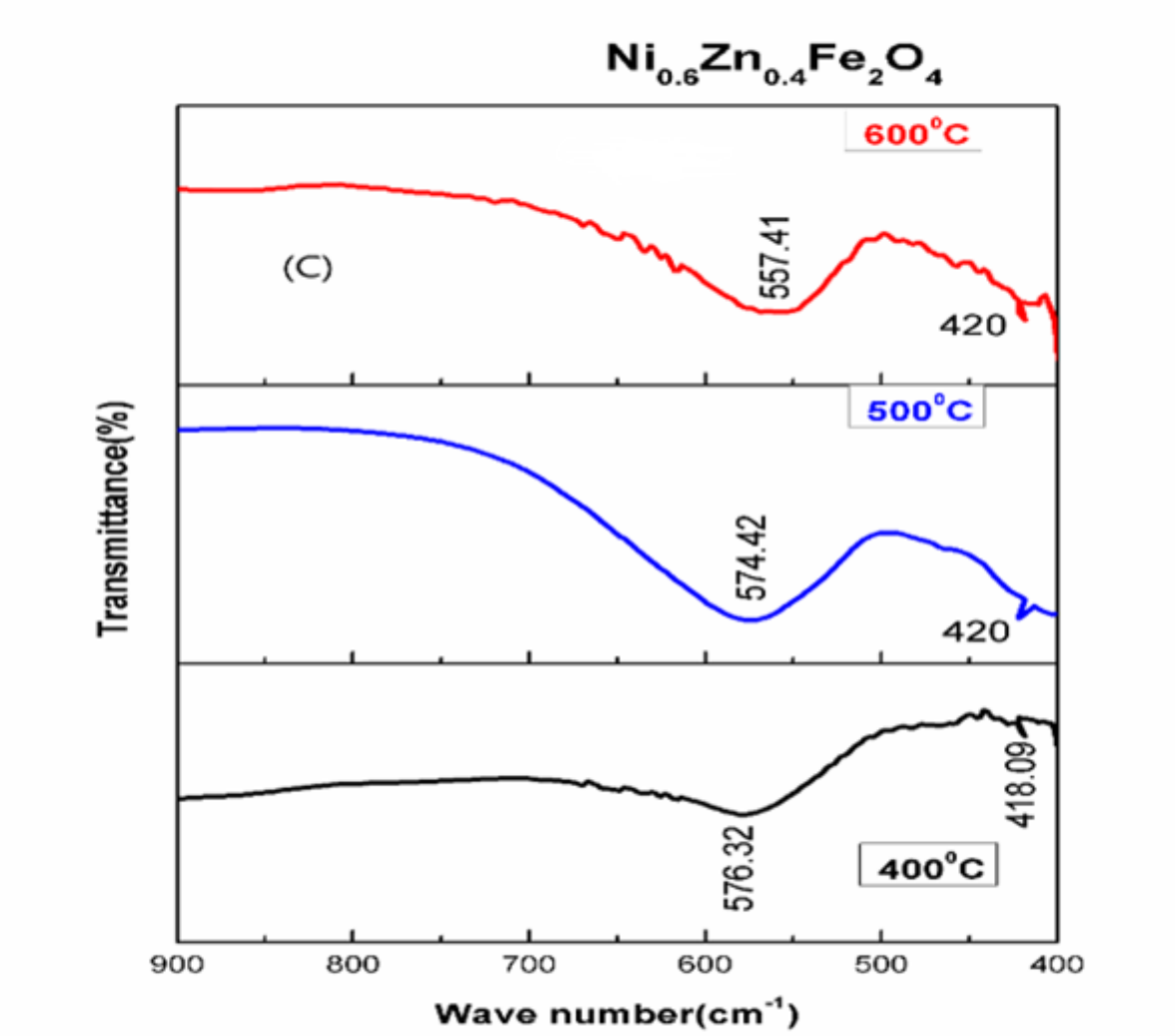

Figure 6

IR spectra for Ni0.6Zn0.4Fe2O4 nano ferrite specimens calcined at 4000C, 5000C and 6000C

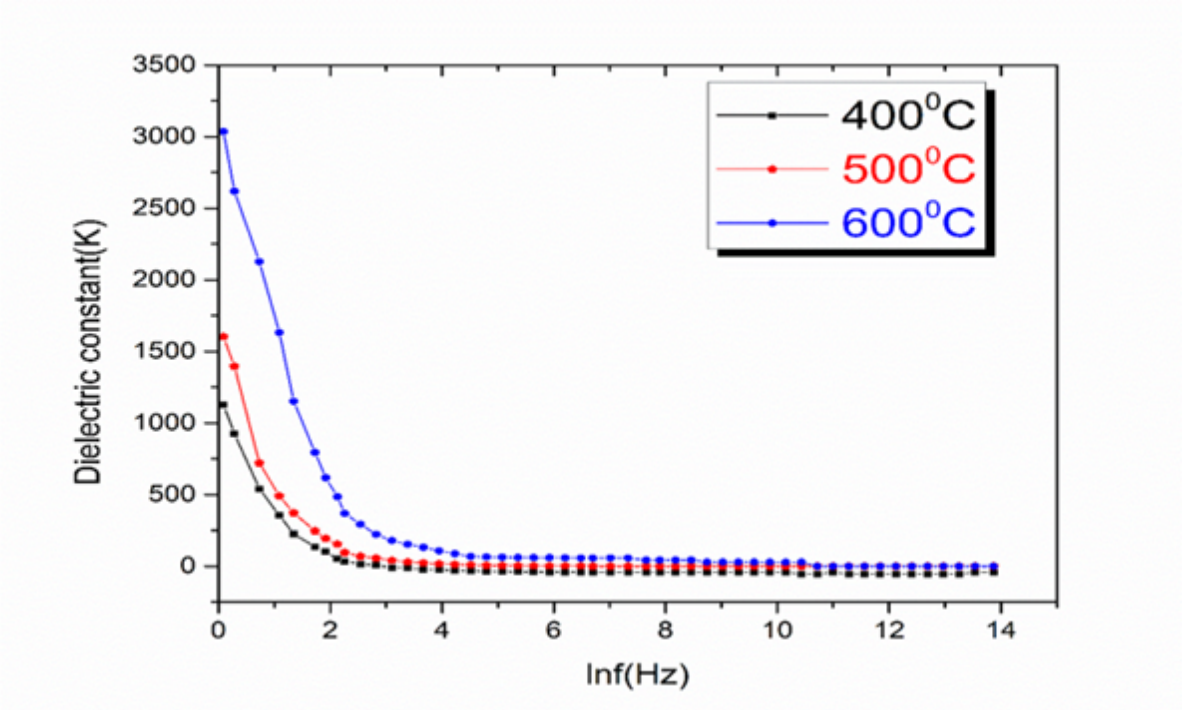

Figure 7

Variation of the dielectric constant of Ni0.6Zn0.4Fe2O4 ferrite nanoparticles calcined at 4000C, 5000C and 6000C.

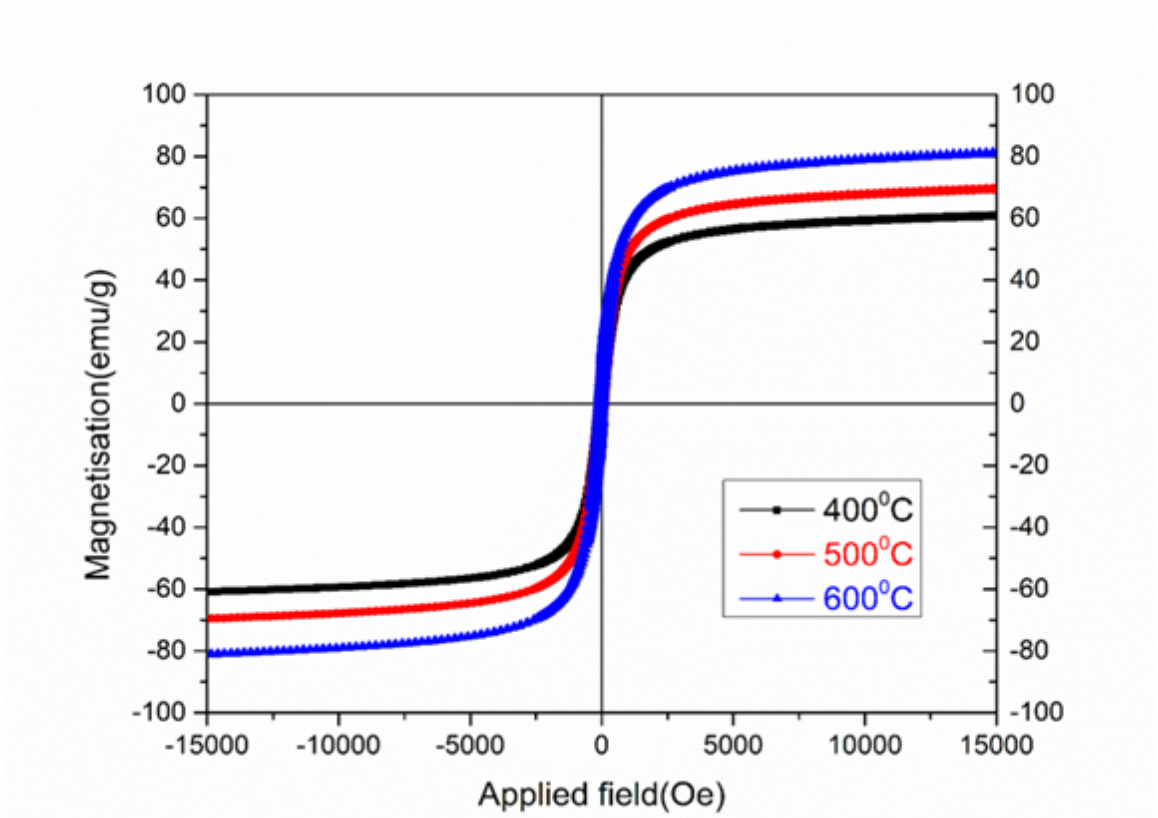

Figure 8

Loading [MathJax]/jax/output/CommonHTML/jax.js articles calcination at 4000C, 5000C and 6000C.

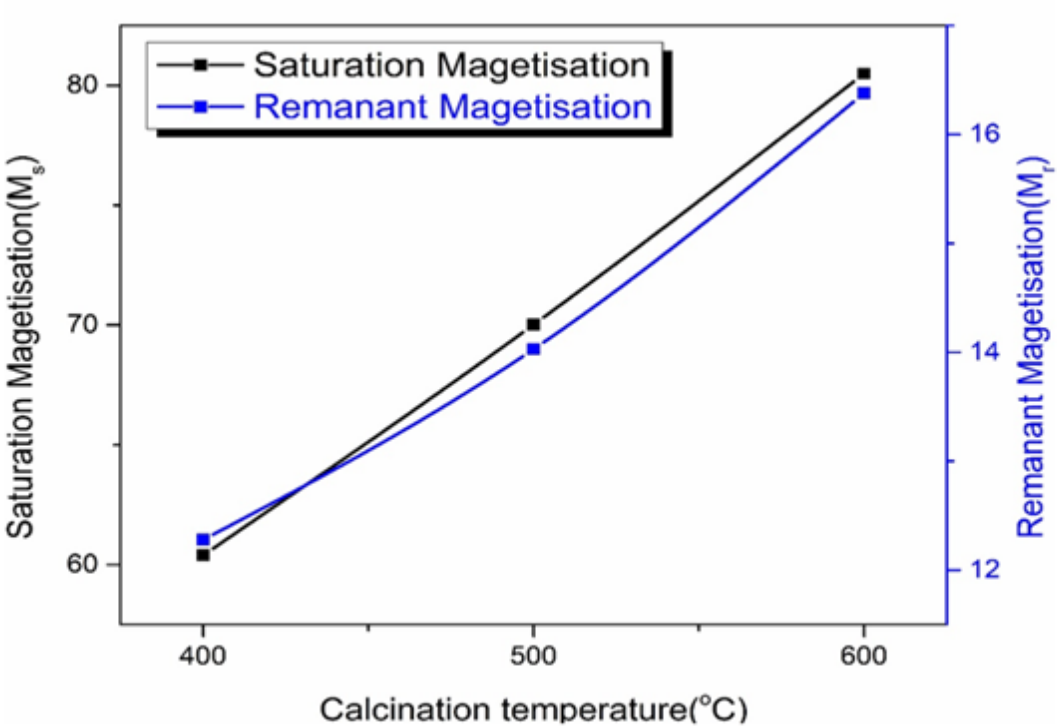

Figure 9

Variation of Ms and Mr values of Ni0.6Zn0.4Fe2O4 ferrite nanoparticles calcination at 4000C, 5000C and 6000C.

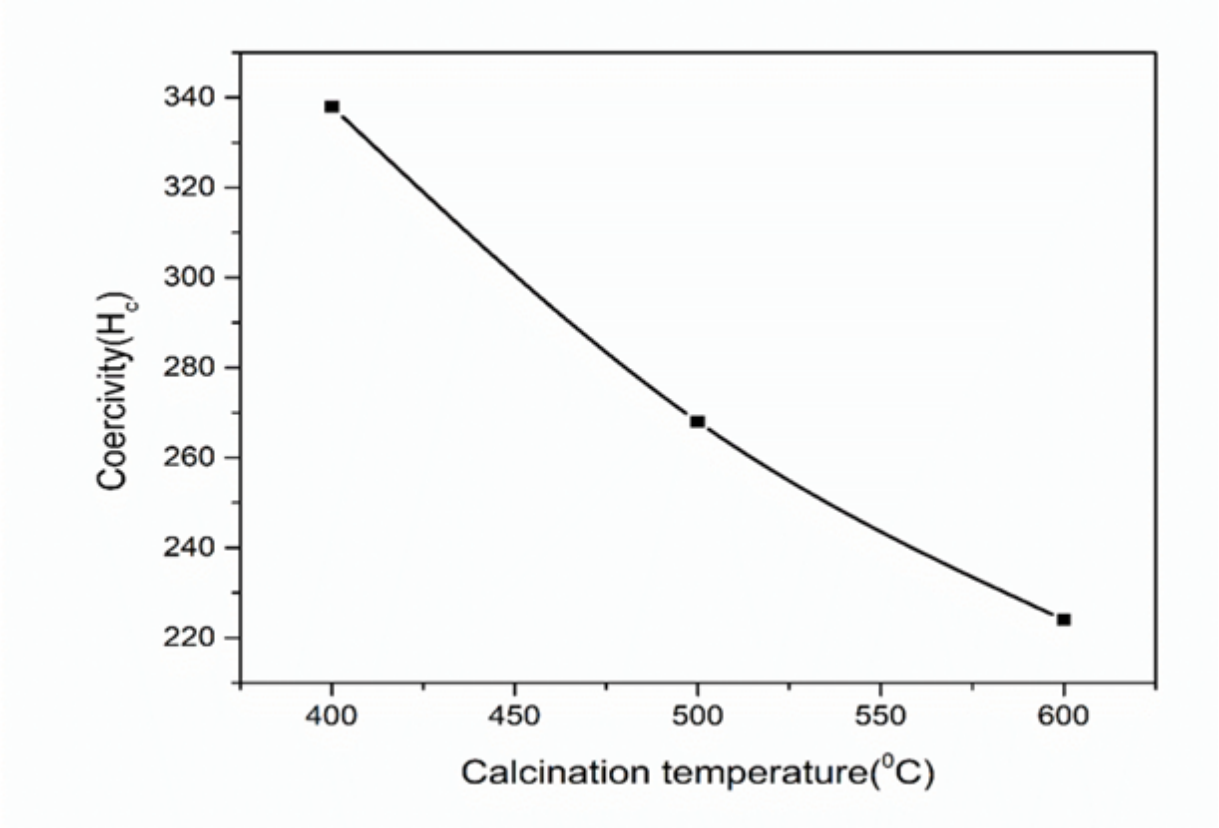

Variation Hc values of Ni0.6Zn0.4Fe2O4 ferrite nanoparticles calcination at 4000C, 5000C and 6000C.